Phyton-
International Journal of
Experimental Botany

Tech Science Press

http://doi.org/10.32604/phyton.2026.080612

ARTICLE

Seed Morphological Changes Associated with the Domestication of *Vitis* Cultivars

José Luis Rodríguez-Lorenzo[1], José Javier Martín-Gómez[2], Ángel Anocibar Beloqui[3], Félix Cabello Sáenz de Santamaría[4], Gregorio Muñoz Organero[4], Ángel Tocino[5] and Emilio Cervantes[2,*]

[1]Plant Developmental Genetics, Institute of Biophysics v.v.i, Academy of Sciences of the Czech Republic, Královopolská 135, Brno, Czech Republic
[2]Instituto de Recursos Naturales y Agrobiología de Salamanca (IRNASA), Consejo Superior de Investigaciones Científicas (CSIC), Cordel de Merinas, 40, Salamanca, Spain
[3]Abadía Retuerta, Sardón de Duero, Spain
[4]Instituto Madrileño de Investigación y Desarrollo Rural Agrario y Alimentario (IMIDRA), Finca El Encín, Alcalá de Henares, Spain
[5]Departamento de Matemáticas, Facultad de Ciencias, Universidad de Salamanca, Plaza de la Merced 1-4, Salamanca, Spain
*Corresponding Author: Emilio Cervantes. Email: emilio.cervantes@irnasa.csic.es

Received: 12 February 2026; Accepted: 25 May 2026; Published: 29 June 2026

ABSTRACT: Background: The transition from wild *Vitis vinifera* subsp. *sylvestris* to cultivated grapes led to major changes in seed shape, known as the "domestication syndrome." While traditional measurements distinguish these groups, high-resolution geometric analysis provides a more precise way to track domestication and variety stability. **Objective:** This study uses a multi-parametric approach—combining Fourier descriptors, curvature analysis, and the $\mathcal{J}$-Index—to quantify seed shape variation across 121 *Vitis* populations. **Methods:** We analysed 48 varieties, including wild species and three major cultivated lineages (Iberian, Central European, and Muscat). **Results:** Principal Component Analysis (PCA) successfully separated wild and cultivated groups. The first three components explained 79% of the variation, driven mainly by seed elongation and curvature. The $\mathcal{J}$-Index proved to be a highly stable metric; it remained consistent across different harvest years (2020–2025) for 'Hebén' and across different locations for 'Cabernet Sauvignon.' Cultivated seeds showed a consistent decrease in solidity and a significant increase in lateral curvature compared to wild seeds. **Conclusion:** Our findings confirm that the $\mathcal{J}$-Index is a robust tool for identifying grapevine varieties. The stability of these geometric traits across different years and environments suggests that clonal propagation effectively "freezes" the morphological identity of grapevine lineages.

KEYWORDS: Convexity; curvature; ferals; morphometry; seeds; solidity; viticulture

1 Introduction

Vitis vinifera L. is one of the most culturally and economically significant crops globally, with over 7 million hectares under cultivation [1,2]. While thousands of cultivars exist, a small group of varieties—such as the Spanish Airén and Tempranillo, or the French Cabernet Sauvignon and Chardonnay—dominates international production [3,4]. A central challenge in viticultural research remains the accurate characterization of these cultivars and the reconstruction of their complex histories. While molecular techniques have revolutionized the field, morphometric approaches provide a vital phenotypic complement for understanding the "domestication syndrome" [5].

The genus *Vitis* presents a complex evolutionary landscape marked by a shift from dioecy in wild populations to hermaphroditism in domesticated vines. Centuries of vegetative propagation have preserved the genetic signatures of ancient cultivars while maintaining high levels of heterozygosity. Significant progress in resolving these lineages was made through microsatellite (SSR) and single nucleotide polymorphism (SNP) markers [6–15], which identified foundational ancestors such as Gouais Blanc, Muscat of Alexandria, Pinot Noir, and Hebén. Pangenome sequencing of 3525 accessions by Dong et al. [16] defined six primary genomic haplotype groups (CG) aligned with eco-geographic origins: the Muscat group (CG3), Balkan varieties (CG4), Western European wine grapes (CG5), and Iberian varieties (CG6). Recent pangenome studies further reveal that structural variants are key drivers of this diversification [17].

Recent studies have shown that seed shape reflects these genetic groupings. The domestication process typically involves a transition from the small, rounded seeds of wild *V. vinifera* subsp. *sylvestris* toward the elongated, piriform shapes found in cultivated varieties [18]. This shift is primarily captured by two metrics: aspect ratio (representing elongation) and solidity (representing the smoothness of the seed outline). For instance, cultivars related to the Iberian 'Hebén' (CG6) display an intermediate morphotype, while "advanced" cultivars in the Muscat group (CG3) exhibit the most extreme elongation and lowest solidity [18–20].

Despite these advances, two gaps remain: the need for a standardized method to quantify seed curvature and the difficulty in distinguishing true *sylvestris* from "feral" individuals (domesticated escapes) using molecular data alone. Elliptic Fourier Analysis (EFA) provides a mathematical framework to address this by reconstructing average outlines across populations [21–23]. In this study, we refine this framework by analyzing 121 *Vitis* populations across four morphotype groups: wild species, and three cultivated lineages corresponding to the groupings by Dong et al. [16] (CG3, CG5, and CG6). By integrating the $\mathcal{J}$-Index [18–20] with curvature analysis [24,25], we aim to validate a multi-parametric method for varietal identification.

We hypothesize that curvature and solidity metrics allow consistent discrimination between wild, cultivated, and feral groups. We propose that these geometric markers provide a stable taxonomic signal, conserved across diverse environments and years, which complements current genomic classifications.

2 Materials and Methods

2.1 Plant Material and Seed Sampling

This study analysed 121 seed samples representing 48 distinct varieties or species within the genus *Vitis*. Detailed information regarding the origin of each sample and its taxonomic classification is provided in Table 1. Of these, seven accessions correspond to *Vitis* species other than *V. vinifera*. Twenty-one samples represent wild-type populations, categorized here as *sylvestris*. These samples were obtained from female vines surveyed between 2003 and 2009 in riparian forests across various locations in France and Spain and subsequently maintained at the IMIDRA germplasm collection. We acknowledge the potential for genomic overlap in these populations; thus, our "sylvestris" category includes both *V. vinifera* subsp. *sylvestris* and potential feral individuals (cultivars escaped from cultivation) that exhibit wild-type morphological traits.

Table 1: List of cultivars and varieties in this work. Superscript indicate the provenances of the seeds: 1, IMIDRA 2020; 2, IMIDRA 2024; 3, IMIDRA 2025; 4, Bodegas Abadía Retuerta, Sardón de Duero (Valladolid, Spain), 2025; 5, Jardín Ampelográfico de Valbusenda, Toro (Zamora, Spain); 6, Bodegas Ayuso, Villarrobledo (Albacete, Spain), 2025. Between Brackets is indicated the adscription to a group: (1) *Vitis* not *V vinifera*, (2) Wild *Vitis vinifera* subsp. *sylvestris* (3) In the pedigree of Hebén, (4) In the pedigree of Savagnin (Traminer), (5) Muscat. Uppercase "b" indicates that two independent samples of Imperial were analysed.

Afus Ali[1,5] (5)	Sumoll[1,2] (3)
Airén[1,6] (3)	*Sylvestris* BA2.3[1] (2)
Albillo Mayor[1,4] (3)	*Sylvestris* CA13.3[1] (2)
Aledo[1,5] (5)	*Sylvestris* CA13.4[1] (2)
Alfrocheiro[1,5] (4)	*Sylvestris* CA13.6[1] (2)
Alphonse Lavallée[1,5] (5)	*Sylvestris* CA2.9[1] (2)
Cabernet Sauvignon[1,4,5,6] (4)	*Sylvestris* CA2.9b[1] (2)
Cardinal[1,5] (5)	*Sylvestris* CC1.5[1] (2)
Cayetana Blanca[1,2] (3)	*Sylvestris* CO4.7[1] (2)
Chenin Blanc[1,5] (4)	*Sylvestris* FR1.1[1] (2)
Gewuertztraminer[1,4,5] (4)	*Sylvestris* FR1.4[1] (2)
Godello[1,4,5] (4)	*Sylvestris* H6.1[1] (2)
Heben[1,2,3] (3)	*Sylvestris* H6.5[1] (2)
Imperial[1,1b] (5)	*Sylvestris* J1.4[1] (2)
Italia[1,5] (5)	*Sylvestris* J2.4[1] (2)
Jaén tinto[1,2] (3)	*Sylvestris* NA2.4b[1]
Koenigin der Weingaerten[1,3] (5)	*Sylvestris* NA3.2b[1] (2)
Marselan[5,5b] (5)	*Sylvestris* S3.5b[1] (2)
Mencía[1,4] (4)	*Sylvestris* SE2.1[1] (2)
Merseguera[1,2] (3)	*Sylvestris* SE2.4[1] (2)
Miguel de Arco[1,2,5] (3)	*Sylvestris* SE2.6[1] (2)
Mollar Cano[1,2,3] (3)	*Sylvestris* SE2.7[1] (2)
Montúa[1,2] (3)	Tarragoní[1,2] (3)[1] (2)
Moscatel de Angués[1,2] (5)	Trepat[1,2] (3)[1]
Muscat a Petit Grains Blancs[1,5] (5)	Verdejo de Rueda[1,4] (4)
Muscat Hamburg[1,3,5] (5)	Verdejo de Salamanca[1,2] (3)
Pedro Ximénez[1,2,5] (3)	*Vitis amurensis*[1] (1)
Pinot Noir[1,4] (4)	*Vitis berlandieri*[1] (1)
Planta Fina[1,2] (3)	*Vitis californica*[1] (1)
Quigat[1,2] (3)	*Vitis candicans*[1] (1)
Red Globe[1,5] (5)	*Vitis doaniana*[1] (1)
Riesling[1,4] (4)	*Vitis riparia*[1] (1)
Sabro[1,2] (3)	*Vitis rupestris*[1] (1)
Sauvignon Blanc[1,4,5] (4)	Xarello[1,2] (3)
Señá[1,2,2b] (3)	

2.1.1 Cultivar Selection and Genetic Clustering

To facilitate comparative analysis, the 121 samples were categorized into five distinct groups based on their taxonomic status and established genetic lineages:

- Group 1: Wild *Vitis* species (Outgroup). This group consists of seven non-*vinifera* species: *V. amurensis*, *V. berlandieri*, *V. californica*, *V. candicans*, *V. doaniana*, *V. riparia*, and *V. rupestris*. These were included as a morphological outgroup to establish the range of seed variation across the genus *Vitis* and to provide a comparative baseline for the *vinifera* lineage.
- Group 2: Wild *Vitis vinifera* subsp. *sylvestris*. This group includes the 21 samples surveyed from riparian forests in France and Spain. As previously noted, this group represents the wild phenotypic spectrum, potentially including both ancestral *sylvestris* lineages and naturalized feral individuals.

- Group 3: Iberian Cultivars (CG6). Cultivars associated with chloroplast haplotype CG6 [16], representing the traditional varieties of the Iberian Peninsula.
- Group 4: Central European Cultivars (CG5). Cultivars associated with chloroplast haplotype CG5 [16], representing the core lineages of Central European viticulture.
- Group 5: Muscat Group (CG3). Cultivars associated with chloroplast haplotype CG3 [16], representing the distinct Muscat lineage characterized by unique aromatic profiles and specific seed morphotypes.

Assignment to these groups was determined either by the documented haplotype of the cultivar [16] or through established pedigree analysis showing direct descent from these foundational lineages [3,9,10,12,13,19].

2.1.2 Provenance and Harvest Standardization

To account for potential environmental and temporal variation in seed development, samples were harvested across multiple years and locations. Seeds were collected from the IMIDRA collection during the 2020 (label 1), 2024 (2), and 2025 (3) seasons. Additional samples were harvested in 2025 from three distinct Spanish viticultural sites to broaden the dataset's environmental representation: Abadía Retuerta (Sardón de Duero, Valladolid), Jardín Ampelográfico de Valbusenda (Toro, Zamora), and Bodegas Ayuso (Villarrobledo, Albacete). The specific harvest site and year for each sample are codified in the legend of Table 1.

2.2 Photography

Images were captured with a Sony α5100 24-megapixel camera (Sony Corp., Tokyo, Japan) equipped with an AF-S Micro NIKKOR 60 mm f/2.8G ED lens (Nikon Corp., Tokyo, Japan). To minimize geometric distortion and ensure maximum reproducibility, the focal distance of the objective was held constant at an object distance of 17 cm, with all specimens positioned strictly in the center of the frame. Each seed was oriented with its ventral side facing the objective. The longitudinal axis—defined by the line connecting the apex and the stalk base—was precisely aligned with the vertical Y-axis of the image field. This standardized orientation is a critical prerequisite to ensure consistency in subsequent elliptical Fourier descriptors and curvature landmark analyses. Camera settings were configured manually to optimize image quality and depth of field, utilizing a shutter speed of 1/5 s, an aperture of f/18, and an ISO sensitivity of 100. Lighting conditions were maintained between 800 and 1200 lumens with a color temperature of 6400 K. No optical or digital noise-reduction filters were applied during or after image acquisition, as the low ISO values ($\leq$400) guaranteed negligible electronic noise. Furthermore, chromatic correction was unnecessary since the original images were computationally binarized into high-contrast black contours for shape analysis. The raw image dataset is publicly available repository via Zenodo (see Supplementary Materials).

2.3 General Morphological Measurements

2.3.1 Seed Morphometric Measurements

Quantitative data, including Area (A), Aspect Ratio (AR), and Solidity (S), were obtained for 20–30 seeds per cultivar using ImageJ v.1.54h [26].

Aspect Ratio (AR) is the ratio of the major axis (L) to the minor axis (W) of the image: $AR = \frac{L}{W}$

Solidity (S) is the ratio of the seed area (A) to the area of its convex hull (A_{hull}). It measures the "smoothness" of the perimeter: $S = \frac{A}{A_{hull}}$

2.3.2 Spatial Calibration and Image Processing

To ensure accuracy in measurements, spatial calibration was performed for each image set:

1. Scaling: A physical ruler included in each high-resolution image served as the reference. Using the "Set Scale" function under the "Analyze" menu, pixel distances were converted into millimeters (mm). For example, a mean area of 42,320 pixels for the cultivar *Hebén* (2020) corresponds to a calibrated area of 21 mm^2.
2. Binarization: Images were converted to 8-bit grayscale format. A global threshold was manually adjusted to optimize the contrast between the seed silhouette and the background, ensuring a clean extraction of the seed perimeter.
3. Automated Extraction: Morphological parameters were recorded using the "Analyze Particles" function, which automatically calculates geometric indices based on the binarized outlines.

2.3.3 Geometric Indices

- Aspect Ratio (AR): Calculated as the ratio of the major axis to the minor axis of the fitted ellipse, representing the degree of elongation.
- Solidity (S): Solidity is a measure of the geometric "density" or convexity of a plane figure. It is defined as the ratio of the actual area of the seed (A) to the area of its convex hull (the smallest convex polygon that entirely encloses the object) [27]. A perfectly convex shape has a Solidity of 1. In this study, Solidity values are expressed as ×1000 to facilitate statistical comparison of fine-scale marginal variations.

2.4 Fourier Equations and Extraction of Fourier Coefficients from the Images with Momocs

Seed outlines are treated here as closed-plane curves, and, as such, may be approximated using sums of trigonometric functions as truncated Fourier expansions [28,29]. When the parametric components are piecewise linear functions $x(t) = \sum_{i=1}^{K} \Delta x_i, y(t) = \sum_{i=1}^{K} \Delta y_i$, these expansions are:

$$X_N(t) = A_0 + \sum_{n=1}^{N} a_n \cos\left(\frac{2n\pi t}{T}\right) + b_n \sin\left(\frac{2n\pi t}{T}\right), \tag{1}$$

$$Y_N(t) = C_0 + \sum_{n=1}^{N} c_n \cos\left(\frac{2n\pi t}{T}\right) + d_n \sin\left(\frac{2n\pi t}{T}\right), \tag{2}$$

where A_0 and C_0 represent the centroid coordinates, and each addend corresponds to an ellipse (the n-th harmonic) determined by the coefficients a_n, b_n, c_n, d_n, which are calculated as:

$$a_n = \frac{T}{2\pi^2 n^2} \sum_{p=1}^{K} \frac{\Delta x_p}{\Delta t_p} \left(\cos\left(\frac{2n\pi t_p}{T}\right) - \cos\left(\frac{2n\pi t_{p-1}}{T}\right) \right), \tag{3}$$

$$b_n = \frac{T}{2\pi^2 n^2} \sum_{p=1}^{K} \frac{\Delta x_p}{\Delta t_p} \left(\sin\left(\frac{2n\pi t_p}{T}\right) - \sin\left(\frac{2n\pi t_{p-1}}{T}\right) \right), \tag{4}$$

$$c_n = \frac{T}{2\pi^2 n^2} \sum_{p=1}^{K} \frac{\Delta y_p}{\Delta t_p} \left(\cos\left(\frac{2n\pi t_p}{T}\right) - \cos\left(\frac{2n\pi t_{p-1}}{T}\right) \right), \tag{5}$$

$$d_n = \frac{T}{2\pi^2 n^2} \sum_{p=1}^{K} \frac{\Delta y_p}{\Delta t_p} \left(\sin\left(\frac{2n\pi t_p}{T} \right) - \sin\left(\frac{2n\pi t_{p-1}}{T} \right) \right). \quad (6)$$

The coefficients a_n, b_n, c_n, d_n of EFT equations can be extracted automatically with the software Momocs [21]. The number N of harmonics determines the degree of precision in the adjustment of the closed curve to the image outline and it may vary depending on the objectives of the study as well as on the characteristics of the image under analysis. While the low-order coefficients ($a_i, b_i, c_i, d_i, i = 1, 2$) define the basic structure of the curves, the higher-order coefficients ($a_i, b_i, c_i, d_i, i > 4$) are responsible for surface details. In addition, b and c coefficients determine the symmetry of the curve. Curves with bilateral symmetry may have $b_i, = d_i = 0, i = 1, 2, \ldots$

Images (JPG) containing 20–30 seeds were converted into .TPS files, the coordinates for seed outline extracted, and the corresponding coefficients were obtained following the protocol outlined in Momocs v1.4.0 [21]. The coefficients were applied to Mathematica equations to determine the average outlines (Aos) relative to each of the seed populations. In the parametric equations representing the curves, coefficients belonging to N = 6 harmonics were considered for curvature analysis. The values $a_1 = 1$, $b_1 = c_1 = 0$ were fixed, thus leaving a total of $6 \times 4 - 3 = 21$, varying coefficients. Equations with 21 varying coefficients defined the Aos that served to calculate curvatures. Although it was estimated that N = 7 accounts for 95% of the total of shape variation in *Vitis* [22,23], and values over it resolve details of the outlines in particular cultivars, for curvature analysis N = 6 results in 10 points well conserved in most cultivars and varieties simplifying the comparisons. In the models N is variable between 7 and 9, giving 4N − 3 coefficients.

2.5 Curvature Analysis

Seed outlines were reconstructed using Elliptic Fourier Descriptors (EFD). Curvature analysis was performed on average outlines derived from Fourier coefficients calculated for six harmonics. This level of approximation was selected to achieve an optimal equilibrium between morphological fidelity and computational simplicity. While increasing the number of harmonics improves the resolution of fine-scale irregularities, it also generates a higher density of curvature points that complicates direct inter-varietal comparisons. At six harmonics, the fundamental geometric structure of the *Vitis* seed—characterized by ten primary curvature extrema—is consistently captured across all accessions, facilitating a standardized comparative framework (see Fig. 1 and Supplementary Materials).

To simplify the geometric model and account for the bilateral symmetry of the seed, the ten detected curvature points were reduced to six representative values:

1. Unique Points: Points 1 (Apex) and 6 (Base) are unique landmarks. Point 1 consistently represents the maximum positive curvature value across all samples.
2. Symmetric Pairs: The remaining eight points were treated as four bilateral pairs. Average values were calculated for points 2/2′, 3/3′, 4/4′, and 5/5′, and assigned as values 2, 3, 4, and 5, respectively.
3. Minimum Curvature: Value 2 (the mean of the 2/2′ pair) typically yields a negative curvature, representing the minimum curvature (inflection zones) of each outline.

The final dataset, comprising the six curvature values, average curvature and curvature ratio (Max to average) and the three morphological indices (A, AR, S), is detailed in Table S1.

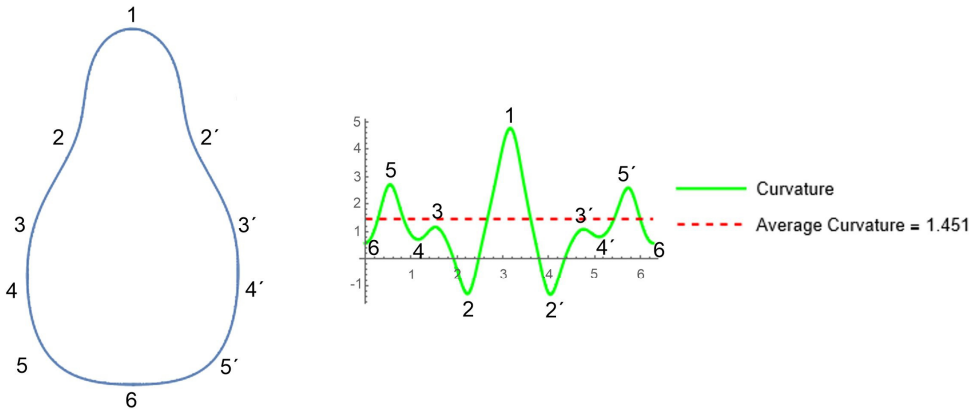

Figure 1: Left: Seed outline resulting from the representation of a Fourier equation with 6 harmonics. Right: 10 notable points of curvature conserved in the cultivars.

2.6 Models and J-Index Measurements

The $\mathcal{J}$-Index was employed to quantify the percentage of geometric similarity between a seed's digital outline and a reference model. This index provides a robust measure of how closely an individual accession adheres to a generalized cultivar or population "archetype."

2.6.1 Model Definition and Standardization

Reference models were created by calculating the arithmetic mean of the Fourier coefficients (a_n, b_n, c_n, d_n) from all populations within a group (e.g., the "Hebén model"). Reference models were developed at two hierarchical levels using Elliptic Fourier Descriptors (EFDs):

- Population Models: For each sample, a specific geometric model was generated using the corresponding Elliptic Fourier equations, utilizing between 6 and 9 harmonics to ensure an accurate representation of the mean population shape.
- Cultivar Models: For cultivars represented by multiple accessions, models were constructed by calculating the arithmetic mean of the Fourier coefficients (a_n, b_n, c_n, d_n) from all constituent populations. This ensured that the resulting "consensus" outline represented the centroid of the cultivar's morphospace.

To ensure consistency during image processing, seed orientation was standardized by aligning the longitudinal axis (the line connecting the apex and the base) with the vertical Y-axis of the image field.

2.6.2 Image Processing and Calculation Protocol

The comparison between seed outlines and reference models followed a standardized digital protocol to ensure maximum alignment (Fig. 2):

- Superimposition: Using Corel PhotoPaint v.24.5 (Corel Corporation, Ottawa, ON, Canada), reference models were superimposed onto the individual seed outlines. Unlike standard rigid-body transformations, this protocol permitted adjustments in the aspect ratio to optimize the fit between the model and the sample, focusing the analysis on the underlying geometric curvature rather than absolute dimensions.
- Area Measurement: Two distinct files were generated for each superimposition: one with the model perimeter in black and one in white. Using ImageJ v.1.53 [26], two area values were recorded:

- Total Area (T): The total surface occupied by the union of the seed and the model (logical OR operation).
- Shared Area (S): The surface area where the seed and the model overlap (logical AND operation).

- The $\mathcal{J}$-Index is a measure of percentage similarity between a seed's outline and a reference model. It is not a black-box metric but a calculation of area overlap. The $\mathcal{J}$-Index is defined as:

$$J\text{-Index} = \frac{S}{T} \times 100,$$

where a score of 100 indicates a perfect geometric match.

Figure 2: Schematic representation of the protocol to measure $\mathcal{J}$-Index (the percent of similarity between a seed and a given model). From left to right: The model, a seed, region of the seed (gray) with the superimposed model showing total area (T), and finally the image in red representing the area shared between the image and the model (S).

2.6.3 Methodological Reliability and Reproducibility

To address inter-operator reproducibility, a subset of 100 seeds was processed independently by two different researchers. The resulting $\mathcal{J}$-Index values showed a high correlation ($R^2 > 0.96$), indicating that the manual alignment protocol in Corel PhotoPaint is robust and highly reproducible. Intra-sample repeatability was assessed by measuring a single population three times on different days, resulting in a coefficient of variation (CV) of less than 2%.

All raw images and superimposition files are archived and accessible via Zenodo (see Supplementary Materials).

2.7 Methodological Pipeline

The workflow followed a four-step sequence:

1. Image Capture: Standardized orientation (ventral view, vertical axis).
2. Pre-processing: Binarization and EFA coefficient extraction via *Momocs*.
3. Shape Quantification: Calculation of curvature points (P1–P6) and the J-Index via area overlap.
4. Statistical Integration: Multivariate analysis (PCA) to distinguish between groups

2.8 Statistics

The dataset for each seed population comprised eleven quantitative variables (see Table S1). Eight variables were derived from the reconstructed average outlines: curvature values at six specific points (P1–P6), the average curvature, and the curvature ratio (maximum to average curvature). The remaining three variables—Area (A), Aspect Ratio (AR), and Solidity (S)—represent the mean values calculated from the individual measurements of 20–30 seeds per population.

All statistical analyses were performed using IBM SPSS Statistics v.28 (SPSS Inc., Chicago, IL, USA) and R v.4.2 [30]. The normality of the data was assessed using the Shapiro-Wilk test; as several variables did not follow a Gaussian distribution, non-parametric methods were employed for all group comparisons.

For analyses involving three or more groups (e.g., comparing the five classification groups), the Kruskal–Wallis *H* test was used. Significant results were further investigated using the Campbell and Skillings stepwise comparison procedure to identify specific inter-group differences while controlling for Type I error. For comparisons between two independent populations, the Mann–Whitney *U* test was applied. A Principal Component Analysis (PCA) was conducted in R to visualize the morphometric space and identify the primary variables driving the differentiation between wild and cultivated accessions. Effect sizes for Kruskal–Wallis tests were estimated using epsilon-squared (η^2) calculated as:

$$\eta^2 = \frac{H - k + 1}{n - k}$$

where H is the Chi-Square value, K is the number of groups and n the total number of samples in the comparison.

3 Results

3.1 Variations in Curvature in the Seed Outlines

Vitis seed images typically present a prominent apical pole (stalk) and a broader basal pole, resulting in a modified elliptical outline (Fig. 3).

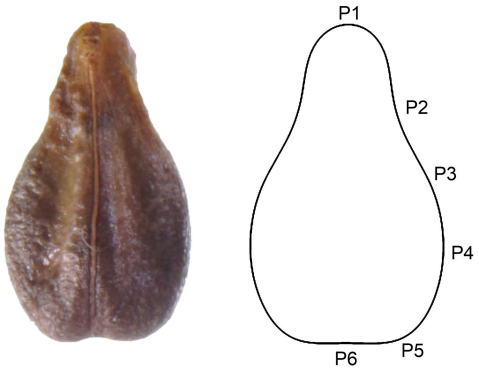

Figure 3: Left: Image of a *Vitis* seed of cultivar Airén (Bodegas Ayuso); Right: Curve from Fourier equation with 8 harmonics. P1: Apex with maximum curvature. P2: Point of negative curvature. P3, P4 and P5 curvature points at the lower lateral surface. P6: Curvature point at the basis.

Reconstructing these outlines using Elliptic Fourier equations with six harmonics captured ten geometric landmarks, reduced to six primary curvature points (P1–P6) for analysis.

The mean values and measures of dispersion across 121 samples are summarized in Table 2. The highest conservation was observed in average curvature (CV = 6.6%) and P5 (CV = 12.0%). In contrast, P6 (basis) and P4 showed the greatest inter-varietal variability (CV > 40%). Cultivars representing the extreme ends of the morphological spectrum are highlighted in Fig. 4. Notably, P2 (negative curvature) reached its minimum absolute value in *V. amurensis* (−0.02) and its maximum in 'Albillo Mayor' (−2.45), representing a critical landmark for domestication tracking.

Table 2: Maximum and minimum values for the curvature values in the seed outlines. Coefficient of variation between brackets.

Measurement	P1 (max)	P2 (min)	P3	P4
Average	5.65 (30.9)	−1.55 (30.1)	1.38 (15.3)	0.41 (44.5)
Maximum score (cultivar)	14.74 (Aledo)	−0.02 (*V. amurensis*)	1.89 (Gewuertztraminer)	0.84 (Jaén Tinto 2024)
Minimum score (cultivar)	2.52 (Cabernet Sauvignon)	−2.45 (Albillo Mayor)	0.91 (Tarragoní 2024)	−0.09 (Chenin Blanc Valb)
Measurement	**P5**	**P6**	**Average**	**Ratio**
Average	2.4 (12)	0.34 (56.8)	1.46 (6.6)	3.9 (31.2)
Maximum score (cultivar)	3.02 (Verdejo de Rueda)	1.61 (Mencía)	1.63 (Chenin Blanc)	9.39 (Aledo)
Minimum score (cultivar)	1.45 (*V. amurensis*)	−0.22 (Afus Ali Valb)	1.12 (*V. amurensis*, *V. candicans*)	1.73 (Cabernet Sauvignon)

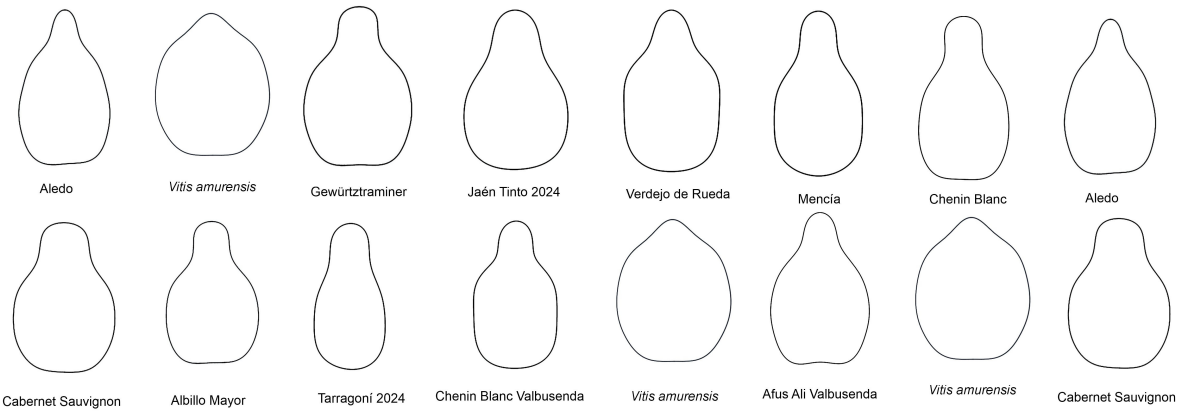

Figure 4: Outlines of the samples having the highest (above) and lowest (below) values of (from left to right) curvature at points P1 to P6, average curvature and ratio maximum to average curvature.

3.2 Factor Reduction by PCA

Principal Component Analysis (PCA) was performed on the eleven morphometric variables (seed size, aspect ratio, solidity, and curvature metrics) across all 121 samples. The analysis identified three principal components accounting for 79% of the total variance.

- PC1 (36.6%): Positively correlated with P2 (negative curvature), solidity, and P4; inversely related to average curvature and P3.
- PC2 (28.4%): Driven by P1 (apex curvature), curvature ratio, area, and P5; inversely related to P6.
- PC3 (14.0%): Associated primarily with aspect ratio and P6 (Table 3).

PERMANOVA results confirmed significant differences between the centroids of the pre-defined groups ($F = 14.17$, $p = 0.001$). However, low silhouette values (ranging from −0.015 for Muscats to 0.124 for wild species) indicate a phenotypic continuum with substantial morphological overlap between groups.

The PCA biplot (Fig. 5) visualizes the distribution of these groups across four quadrants (Q1–Q4). Q4 is largely occupied by wild species and *sylvestris* accessions, characterized by higher solidity and P2 values. Domesticated cultivars are distributed across the remaining quadrants: the *Hebén* group (CG6) predominates in Q1, Muscat types (CG3) in Q2, and the *Traminer* lineage (CG5) in Q3. *Sylvestris* samples

exhibit an intermediate distribution, overlapping with the *Hebén* and *Traminer* groups but notably absent from the *Muscat* cluster.

Table 3: Results of PCA on 121 samples of varieties and cultivars of *Vitis*.

	Component		
	1	**2**	**3**
P2	0.959		
Ave	−0,890		
Sol	0.804		
P4	0.656		
P3	−0.615		−0.590
P5	−0.570	0.626	
P1	0.252	0.836	
Ratio	0.454	0.776	
P6		−0.577	0.589
Area		0.633	
Aspect Ratio	−0.489		0.817

While the significant differences in centroids confirm distinct morphological 'signatures' for each group, low silhouette values confirm a high degree of overlap—consistent with a common genomic background, and a large variation in the groups (phenotypic continuum). The silhouette values oscillated between −0.015 (Muscat group) and 0.124 (*Vitis* no *vinifera* group), thus indicating low separation between the groups. The ellipses of groups sylvestris, Traminer and Hebén are elongated indicating heterogeneity among the samples in these groups. Neverthelelss, there were notable differences among the cultivars offering the possibility to define morphotypes. The samples of Hebén 2020 and 2024 are very close to each other and, in their proximity, there is a good representation of cultivars in the progeny of Hebén (Miguel de Arco, Merseguera, Montúa, Plant Fina, Quigat, Señá, Trepat, Verdejo de Salamanca and Xarello).

The progeny of Savagnin (Traminer) expands to the left in the lower part of the diagram in a region occupied by Chenin Blanc, Gewuertztraminer, Godello, Alfrocheiro, Riesling, Mencía and Pinot Noir, having all these cultivars a related pedigree. Verdejo Blanco, in the progeny of Savagnin and Castellana Blanca, expands to the upper left part of the diagram. In the region between Hebén and Traminer-related cultivars there is a concentration of Muscat-type cultivars, sharing parent-offspring relationships between them, such as Alphonse Lavallee, Cardinal, Imperial, Muscat Hamburg, Muscat a Petits Grains. Afus Ali and Aledo are on top of the diagram with high values of P1 and average curvature.

Those results justify the use of ANOVA to identify specific canalized traits—such as aspect ratio related to seed elongation, solidity or particular variations in curvature points.

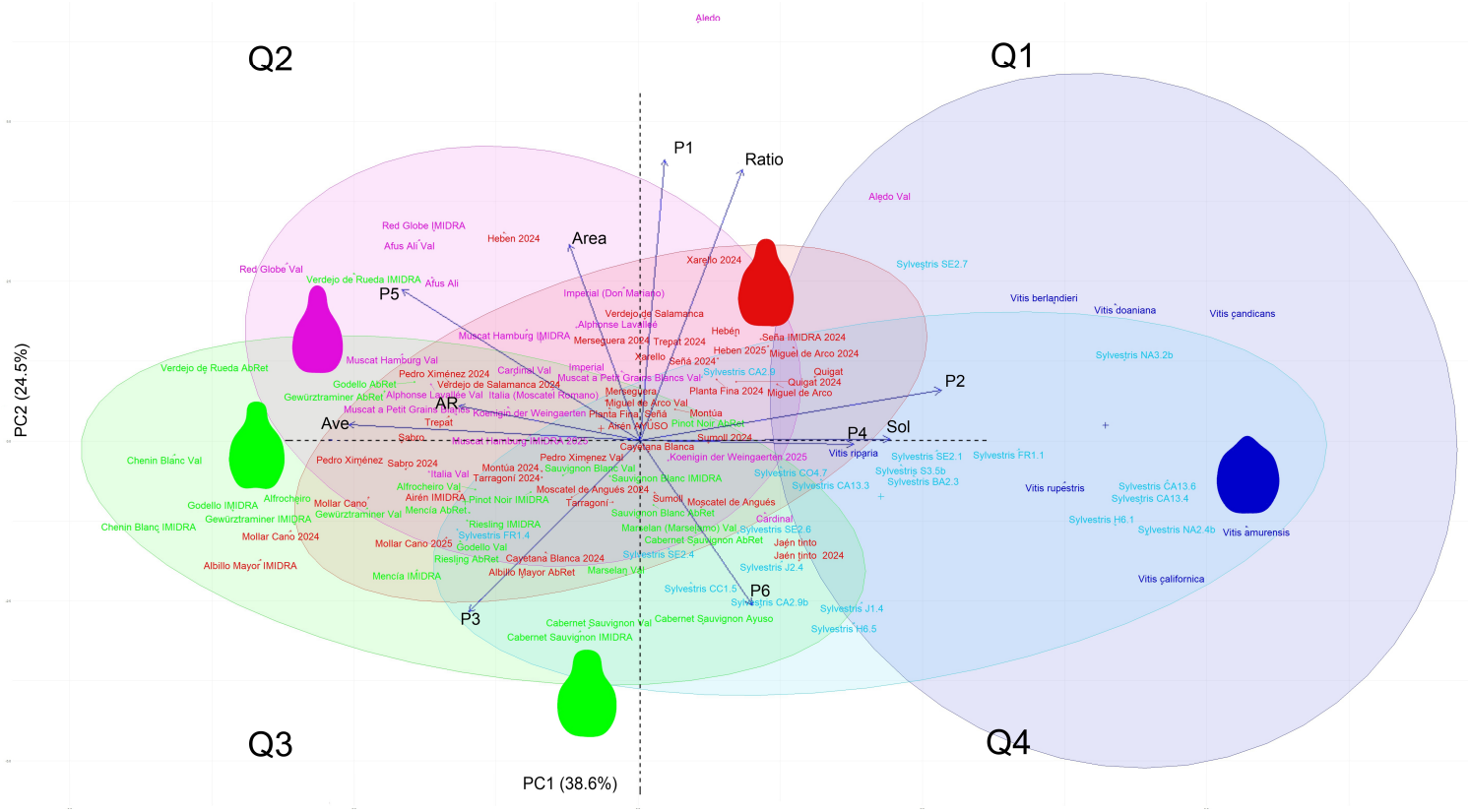

Figure 5: Biplot with the Results of PCA. Dark blue: group of *Vitis* species other than *V. vinifera*; light blue: *sylvestris*; red: Hebén group; purple: muscat. Green: Traminer group. PC1 (Dim1) is related to P2, solidity and P4, and inversely related to average curvature and P3. PC2 (Dim2) is related to P1, curvature ratio, area and P5, and inversely related to P6.

3.3 Comparison between Groups

Significant differences were identified across the groups using Kruskal–Wallis tests (Table 4).

- Group of non-*vinifera* species (Group 1): Characterized by the highest solidity (968.0), lowest aspect ratio (1.36), and lowest average curvature.
- Iberian/Hebén group—CG6 (Group 3): Displayed intermediate solidity (954.6) and P2 values.
- Groups of Traminer (CG5; Group 4): and Muscats (CG3; Group 5): Exhibited the lowest solidity (946.5 and 945.3, respectively) and the highest absolute values for negative curvature (P2).
- Group of Muscats (Group 5): Showed significantly larger seed area (20.1 mm^2) compared to other groups ($p < 0.05$).

Effect sizes were large for all magnitudes except area (moderate).

Table 4: Results of the Kruskal-Wallis test for the comparison of measurements (A, area; AR, aspect ratio; S, solidity) and curvature values between groups 1, 3, 4, and 5. Different letters in superscript in consecutive rows in each column indicate significant differences. Between brackets: coefficient of variation.

Group	N	A	AR	S	P1	P2	P3	P4	P5	P6	Ave	Ratio
Group 1	7	16.8^{a} (13.4)	1.36^{a} (6.4)	968.0^{c} (0.8)	6.32^{bc} (31.2)	-0.50^{c} (71.6)	1.27^{a} (11.6)	0.65^{b} (13.6)	1.75^{a} (11.8)	0.80^{b} (34.0)	1.22^{a} (8.0)	5.15^{c} (28.4)
Group 3	45	17.5^{a} (14.9)	1.66^{b} (7.1)	954.6^{b} (1.0)	5.53^{b} (22.1)	-1.52^{b} (23.1)	1.32^{a} (15.5)	0.40^{a} (40.9)	2.43^{b} (7.9)	0.61^{ab} (48.5)	1.45^{b} (4.2)	3.83^{b} (23.3)
Group 4	27	16.7^{a} (13.6)	1.65^{b} (6.5)	946.5^{a} (1.2)	4.54^{a} (27.8)	-1.79^{a} (20.3)	1.56^{b} (11.6)	0.34^{a} (56.6)	2.48^{b} (11.2)	0.63^{ab} (63.9)	1.49^{c} (4.8)	3.03^{a} (26.4)
Group 5	21	20.1^{b} (20.1)	1.63^{b} (7.7)	945.3^{a} (1.1)	7.13^{c} (29.7)	-1.66^{a} (21.2)	1.33^{a} (12.0)	0.46^{a} (35.9)	2.50^{b} (9.2)	0.46^{a} (72.0)	1.50^{c} (4.5)	4.75^{c} (28.1)
Effect size		0.123	0.352	0.370	0.217	0.343	0.177	0.145	0.477	0.166	0.380	0.245

3.4 Analysis by J-Index

The $\mathcal{J}$-Index quantified the morphological fit between seed samples and reference models for *Cabernet Sauvignon* and *Hebén* (Fig. 6).

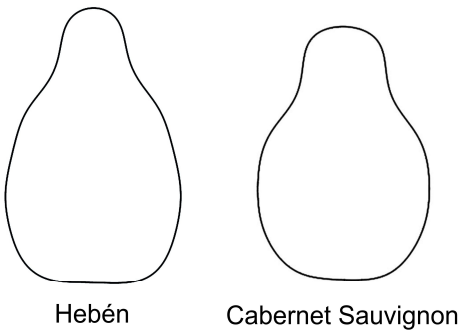

Figure 6: Models for Hebén and Cabernet Sauvignon were made with the average outlines of three and four populations respectively for each cultivar.

- Cabernet Sauvignon Model: Testing against multiple cultivars revealed a significantly higher $\mathcal{J}$-Index for *Cabernet Sauvignon* (92.4%) compared to *Garnacha Tinta* (89.9%) and *Gewuerztraminer* (89.8%) (Table 5).

Table 5: *J*-Index values for the comparison of seed images of the cultivars Cabernet Sauvignon, Garnacha Tinta, Gewuertztraminer and Sauvignon Blanc. Different letters in superscript in consecutive rows in each column indicate significant differences. Between brackets: coefficient of variation.

Cultivar	N	*J*-Index with Model Cabernet Sauvignon	Confidence Interval (95%)
Cabernet Sauvignon	80	92.4^{c} (1.5)	92.1–92.7
Garnacha Tinta	60	89.9^{a} (2.3)	89.3–90.4
Gewuertztraminer	60	89.8^{a} (2.3)	89.2–90.3
Sauvignon Blanc	60	90.8^{b} (2.7)	90.2–91.4

- Hebén Model: This model successfully identified *Hebén* (92.1%) and its direct progeny, *Mollar Cano* (92.1%), showing no significant difference between the two. However, it significantly discriminated against the more morphologically distant *Muscat Hamburg* (88.6%) and *Gewuerztraminer* (90.9%) (Table 6).

Table 6: *J*-Index values for the comparison of seed images of the cultivars Gewuertztraminer, Hebén, Mollar Cano and Muscat Hamburg with the model Hebén. Different letters in superscript in consecutive rows in each column indicate significant differences. Between brackets: coefficient of variation.

Cultivar	N	*J*-Index with Model Hebén	Confidence Interval (95%)
Gewuertztraminer	60	90.9^{b} (2.4)	90.4–91.5
Hebén	60	92.1^{c} (1.9)	91.6–92.6
Mollar Cano	60	92.1^{c} (1.3)	91.8–92.4
Muscat Hamburg	60	88.6^{a} (3.3)	87.8–89.3

4 Discussion

4.1 Morphometric Indicators of the "Wild Syndrome" and Domestication Trajectories

Discriminating between wild and domesticated *Vitis* seeds has been a central objective of viticultural research for decades [31–36]. The transition from traditional measurements to automated image analysis now allows for a high-resolution characterization of both modern cultivars and fossil remains [23,37–39]. Our results reinforce the concept of the "wild syndrome," characterized by rounded seeds with short stalks and high solidity [22,35,36]. A key finding of this study is the geometric relationship between solidity and negative curvature across *Vitis* species and cultivars. Because solidity represents the ratio of a shape's area to its convex hull, the presence of negative curvature (inflection zones) at the stalk-chalaza intersection directly reduces solidity values. The observed morphometric gradient—extending from the high solidity and minimal negative curvature of *Vitis* species outgroups to the low-solidity, elongated forms of the Muscat and Savagnin groups—suggests a progressive shift in seed geometry. While accessions within the Hebén lineage (CG6) occupy an intermediate morphospace, these results should be interpreted as morphometric tendencies rather than definitive taxonomic classifications. These "transitional" patterns likely reflect cultivars that have retained ancestral morphological features while undergoing different selective pressures than more recently bred varieties.

4.2 Interpreting the Phenotypic Continuum: Wild vs. Feral Populations

A significant portion of our *sylvestris* samples were distributed across the PCA plot, overlapping with both non-*vinifera* species and domesticated cultivars. This high degree of overlap—evidenced by low silhouette values—confirms a phenotypic continuum rather than discrete, isolated clusters. While some

populations may represent true relictual *V. vinifera* subsp. *sylvestris*, the clustering of certain "wild" samples within domesticated quadrants (Q1 and Q3) suggests the presence of "feral" plants (domesticated escapes) or wild-domestic hybrids [40–42]. Because true *sylvestris* is strictly dioecious, the morphological proximity of some wild samples to hermaphroditic cultivars supports the need for a re-evaluation of European wild *Vitis* populations [43,44]. However, these patterns are plausible morphometric inferences and require independent molecular validation. High-throughput sequencing is necessary to confirm whether these similarities stem from shared ancestry, recent introgression, or feralization.

4.3 Morphotypes in Pedigree and Haplotype Context

The morphometric groups defined here show a notable correspondence with the molecularly defined haplotypes (CG3, CG5, CG6) established by Dong et al. [16]. The relative consistency of the *Hebén* (CG6) and *Savagnin* (CG5) progeny clusters suggests that seed geometry can serve as a phenotypic complement to pedigree analysis. For instance, the proximity of 'Mollar Cano' to the 'Hebén' model aligns with its documented parentage [12,13]. Conversely, instances where progeny deviate from the maternal model, such as 'Sabro' or 'Pedro Ximénez', likely reflect the geometric influence of an unknown paternal parent or transgressive segregation.

Furthermore, the $\mathcal{J}$-Index analysis of Hebén and Cabernet Sauvignon highlights the stability of these "morphotypes" across diverse geographic origins. This stability suggests that while environmental factors (such as hot summers or water stress) may alter seed size or aspect ratio [45–47], the underlying geometric "blueprint" defined by curvature and solidity remains relatively conserved during long periods of vegetative reproduction [48].

4.4 Limitations and Future Directions

Despite the clear trends identified, the substantial overlap in the multivariate space remains a primary limitation. This phenotypic continuum suggests that seed shape is subject to significant variation, likely driven by the complex maternal nature of seed tissues and environmental plasticity. Our study highlights morphometric affinities, but these should not be used as a standalone proxy for genetic identity.

Future research should integrate these geometric markers with independent molecular datasets to isolate the specific genetic factors responsible for seed curvature and solidity. By integrating $\mathcal{J}$-Index modeling with curvature analysis, we provide a non-invasive tool that complements molecular data. This approach offers powerful insights into the phenotypic boundaries of *Vitis*, provided it is used within a multidisciplinary framework to decode the evolutionary history of the grapevine.

Acknowledgement: We thank to Miguel Ángel Marino of Jardín Ampelográfico Valbusenda (Toro, Zamora, Spain), María José Jerez Catalán of Bodegas Ayuso Villarrobledo (Albacete, Spain), and personnel of Abadía Retuerta (Sardón de Duero, Valladolid, Spain), for providing seeds. Project "CLU-2025-2-02—Unit of Excellence IRNASA_CSIC", funded by the Junta de Castilla y León and co-funded by the European Union (FEDER "Europe boosts our growth"), and Project "DEEP-MaX-2024_IRNASA" funded by CSIC.

Funding Statement: The authors received no specific funding for this study.

Author Contributions: The authors confirm contribution to the paper as follows: Conceptualization, Emilio Cervantes; methodology, José Luis Rodríguez-Lorenzo, José Javier Martín-Gómez, Ángel Anocibar Beloqui, Félix Cabello Sáenz de Santamaría, Gregorio Muñoz Organero, Ángel Tocino and Emilio Cervantes; software, José Luis Rodríguez-Lorenzo, José Javier Martín-Gómez and Emilio Cervantes; validation, José Luis Rodríguez-Lorenzo, José Javier Martín-Gómez, Ángel Anocibar Beloqui, Félix Cabello Sáenz de Santamaría, Gregorio Muñoz Organero, Ángel Tocino and Emilio Cervantes; formal analysis, José Luis Rodríguez-Lorenzo, José Javier Martín-Gómez and

Emilio Cervantes; investigation, José Luis Rodríguez-Lorenzo, José Javier Martín-Gómez, Ángel Anocibar Beloqui, Félix Cabello Sáenz de Santamaría, Gregorio Muñoz Organero, Ángel Tocino and Emilio Cervantes; data curation, José Luis Rodríguez-Lorenzo, José Javier Martín-Gómez and Emilio Cervantes; writing—original draft preparation, Emilio Cervantes; writing—review and editing, José Luis Rodríguez-Lorenzo, José Javier Martín-Gómez, Ángel Anocibar Beloqui, Félix Cabello Sáenz de Santamaría, Gregorio Muñoz Organero, Ángel Tocino and Emilio Cervantes; visualization, José Luis Rodríguez-Lorenzo, José Javier Martín-Gómez and Emilio Cervantes; supervision, Ángel Tocino and Emilio Cervantes; project administration, Emilio Cervantes; funding acquisition, Emilio Cervantes. All authors reviewed and approved the final version of the manuscript.

Availability of Data and Materials: The authors confirm that the data supporting the findings of this study are available within the article [and/or] its Supplementary Materials.

Ethics Approval: Not applicable.

Conflicts of Interest: The authors declare no conflicts of interest to report regarding the present study.

Supplementary Materials: Images of seeds harvested in IMIDRA in 2020 and 2024 are available at https://zenodo.org/records/15829028, and https://zenodo.org/records/14610754, respectively. Table S1, containing the values of six points of curvature and morphological measurements (A, AR and S) for all populations under study; images of seeds from Abadía Retuerta, IMIDRA, Jardín Ampelográfico Valbusenda and Bodegas Ayuso harvested in 2025; images for $\mathcal{J}$-Index calculations and Mathematica files for curvature analysis are available at: https://zenodo.org/records/18622032.

Glossary

Average outlines (Aos)	Continuous closed curves representing the shape of 20–30 seeds for each of the population under study
Cultivar	Any of the varieties of *Vitis vinifera* subsp. *vinifera* or hybrids traditionally established as a crop for the production of wine or table grapes. A cultivar has been historically bred, or developed by humans for desirable characteristics.
Curvature	Curvature is the rate of change of the tangent in a curve. Mathematically, it's the derivative of the tangent's angle with respect to arc length, often described as the inverse of the radius for a circle (a straight line has zero curvature)
Notable curvature points	Notable curvature points refer to key locations on curves where curvature changes significantly, such as inflection points (where a curve goes from curving left to right, locally straight), cusps (sharp points where direction reverses), vertices, foci, and points of maximum/minimum curvature
Variety	Any of the lines of *Vitis* grown in experimental stations. They can belong to cultivars or to other species of *Vitis* or to *Vitis vinifera* subsp. *sylvestris*.

References

1. Mullins MG, Bouquet A, Williams LE. Biology of the grapevine. Cambridge, UK: Cambridge University Press; 1992.
2. OIV. World statistics: organisation internationale de la vigne et du vin; 2017 [cited 2025 Oct 15]. Available from: http://www.oiv.int/en/statistiques/recherche.
3. Röckel E, Töpfer R, Röckel F, Brühl U, Hundemer M, Mahler-Ries A. *Vitis* international variety catalogue—www.vivc.de—2024. [cited 2025 Oct 4]. Available online: https://www.vivc.de/index.php?r=aboutvivc%2Fdescriptors.
4. Lexicon: the largest wine encyclopedia in the world with 26,513 terms. [cited 2025 Jan 1]. Available online: https://www.vivc.de/.
5. Rodríguez-Lorenzo JL, Janoušek B, Cervantes E. Viticulture: history, breeding systems and recent developments. Phyton. 2025;94(9):2649–67. [CrossRef].

6. Thomas MR, Scott NS. Microsatellite repeats in grapevine reveal DNA polymorphisms when analysed as sequence-tagged sites (STSs). Theor Appl Genet. 1993;86(8):985–90. [CrossRef].
7. Bitz L, Zinelabidine L, Ruehl E, Bitz O. Microsatellite analysis of traditional eastern grapevine varieties and wild accessions from Geisenheim collection in Germany. Vitis. 2015;54:17–21.
8. Ferreira V, Pinto-Carnide O, Mota T, Martín J, Ortiz J, Castro I. Identification of minority grapevine cultivars from vinhos verdes Portuguese DOC region. Vitis. 2015;54:53–8.
9. Laucou V, Lacombe T, Dechesne F, Siret R, Bruno JP, Dessup M, et al. High throughput analysis of grape genetic diversity as a tool for germplasm collection management. Theor Appl Genet. 2011;122(6):1233–45. [CrossRef].
10. Lacombe T, Boursiquot JM, Laucou V, Di Vecchi-Staraz M, Péros JP, This P. Large-scale parentage analysis in an extended set of grapevine cultivars (*Vitis vinifera* L.). Theor Appl Genet. 2013;126(2):401–14. [CrossRef].
11. Milla Tapia A, Cabezas JA, Cabello F, Lacombe T, Martínez-Zapater JM, Hinrichsen P, et al. Determining the Spain origin of representative ancient American grapevine cultivars. Am J Enol Vitic. 2007;58(2):242–51. [CrossRef].
12. Zinelabidine LH, Cunha J, Eiras-Dias JE, Cabello F, Martínez-Zapater JM, Ibáñez J. Pedigree analysis of the Spanish grapevine cultivar 'Hebén'. Vitis. 2015;54:81–6.
13. Zinelabidine LH, Haddioui A, Rodríguez V, Cabello F, Eiras-Dias JE, Martínez-Zapater JM, et al. Identification by SNP analysis of a major role for Cayetana Blanca in the genetic network of Iberian Peninsula grapevine cultivars. Am J Enol Vitic. 2012;63(1):121–6. [CrossRef].
14. Hunt HV, Lawes MC, Bower MA, Haeger JW, Howe CJ. A banned variety was the mother of several major wine grapes. Biol Lett. 2010;6(3):367–9. [CrossRef].
15. Bowers JE, Boursiquot JM, This P, Chu K, Johansson H, Meredith CP. Historical genetics: the parentage of Chardonnay, Gamay, and other wine grapes of Northeastern France. Science. 1999;285(5433):1562–5. [CrossRef].
16. Dong Y, Duan S, Xia Q, Liang Z, Dong X, Margaryan K, et al. Dual domestications and origin of traits in grapevine evolution. Science. 2023;379(6635):892–901. [CrossRef].
17. Liu Z, Wang N, Su Y, Long Q, Peng Y, Shangguan L, et al. Grapevine pangenome facilitates trait genetics and genomic breeding. Nat Genet. 2024;56(12):2804–14. [CrossRef].
18. Martín-Gómez JJ, Rodríguez-Lorenzo JL, Espinosa-Roldán FE, Cabello Sáenz de Santamaría F, Muñoz-Organero G, Tocino Á, et al. Morphometric analysis reveals new data in the history of *Vitis* cultivars. Plants. 2025;14(16):2481. [CrossRef].
19. Cervantes E, Martín-Gómez JJ, Rodríguez-Lorenzo JL, del Pozo DG, Cabello Sáenz de Santamaría F, Muñoz-Organero G, et al. Seed morphology in *Vitis* cultivars related to Hebén. AgriEngineering. 2025;7(3):62. [CrossRef].
20. Martín-Gómez JJ, Rodríguez-Lorenzo JL, Espinosa-Roldán FE, de Santamaría FCS, Muñoz-Organero G, Tocino Á, et al. Seed morphometry reveals two major groups in Spanish grapevine cultivars. Plants. 2025;14(10):1522. [CrossRef].
21. Bonhomme V, Picq S, Gaucherel C, Claude J. Momocs: outline analysis Using R. J Stat Soft. 2014;56(13):1–24. [CrossRef].
22. Bonhomme V, Terral JF, Zech-Matterne V, Ivorra S, Lacombe T, Deborde G, et al. Seed morphology uncovers 1500 years of vine agrobiodiversity before the advent of the Champagne wine. Sci Rep. 2021;11:2305. [CrossRef].
23. Terral JF, Tabard E, Bouby L, Ivorra S, Pastor T, Figueiral I, et al. Evolution and history of grapevine (*Vitis vinifera*) under domestication: New morphometric perspectives. Ann Bot. 2010;105(3):443–55. [CrossRef].
24. Cervantes E, Tocino A. Geometric analysis of Arabidopsis root apex reveals a new aspect of the ethylene signal transduction pathway in development. J Plant Physiol. 2005;162(9):1038–45. [CrossRef].
25. Cervantes E, Martín-Gómez JJ, Espinosa-Roldán FE, Muñoz-Organero G, Tocino Á, Cabello Sáenz de Santamaría F. Seed apex curvature in key Spanish grapevine cultivars. Vitic Data J. 2021;3:e66478. [CrossRef].
26. Ferreira T, Rasband W. ImageJ user guide-Ij1.46r, 186 p. 2012 [cited 2026 Jun 12]. Available from: https://imagej.net/.
27. Gray A. Modern differential geometry of curves and surfaces with mathematica. Boca Raton, FL, USA: CRC Press; 1998. p. 163–5.
28. McLellan T, Endler JA. The relative success of some methods for measuring and describing the shape of complex objects. Syst Biol. 1998;47(2):264–81. [CrossRef].

29. Kuhl FP, Giardina CR. Elliptic Fourier features of a closed contour. Comput Graph Image Process. 1982;18(3):236–58. [CrossRef].
30. R Core Team. R: a language and environment for statistical computing, version 4.1.2. Vienna, Austria: R Foundation for Statistical Computing; 2021.
31. Stummer A. Zur Prehistory of the Grapevine and Winegrowing. Mitteilungen Anthropol. Gessellschaft Wien. 1911;41:283–96. (In German).
32. Levadoux L. Wild and cultivated populations of *Vitis vinifera.* Ann L'Amelior Plantes. 1956;1:59–118. (In French).
33. Terpó A. The carpological examination of wild growing grapevine species of Hungary. I. Qualitative and quantitative characteristics. Acta Bot Hung. 1976;22:209–47.
34. Mangafa M, Kotsakis K. A new method for the identification of wild and cultivated charred grape seeds. J Archaeol Sci. 1996;23(3):409–18. [CrossRef].
35. Rivera D, Valera J, Maghradze D, Kikvadze M, Nebish A, Ocete R, et al. Heterogeneity in seed samples from vineyards and natural habitats along the Eurasian Vitis vinifera range: implications for domestication and hybridization. Horticulturae. 2025;11(1):92. [CrossRef].
36. Obón C, Rivera-Obón DJ, Valera J, Matilla G, Alcaraz F, Maghradze D, et al. Is there a domestication syndrome in Vitis (Vitaceae) seed morphology. Genet Resour Crop Evol. 2025;72(2):1541–65. [CrossRef].
37. Di Cecco V, Manzi A, Zulli C, Di Musciano M, D'Archivio AA, Di Santo M, et al. Study of grapevine (*Vitis vinifera* L.) seed morphometry. Seeds. 2024;3:311–23. [CrossRef].
38. Ucchesu M, Martinetto E, Sarigu M, Orrù M, Bornancin M, Bacchetta G. Morphological characterization of fossil Vitis L. seeds from the gelasian of Italy by seed image analysis. Plants. 2024;13(10):1417. [CrossRef].
39. Bouby L, Wales N, Jalabadze M, Rusishvili N, Bonhomme V, Ramos-Madrigal J, et al. Tracking the history of grapevine cultivation in Georgia by combining geometric morphometrics and ancient DNA. Veg Hist Archaeobot. 2021;30(1):63–76. [CrossRef].
40. D'Onofrio C. Introgression among cultivated and wild grapevine in Tuscany. Front Plant Sci. 2020;11:202. [CrossRef].
41. Zecca G, De Mattia F, Lovicu G, Labra M, Sala F, Grassi F. Wild grapevine: silvestris, hybrids or cultivars that escaped from vineyards? Molecular evidence in Sardinia. Plant Biol. 2010;12(3):558–62. [CrossRef].
42. Zecca G, Labra M, Grassi F. Untangling the evolution of American wild grapes: admixed species and how to find them. Front Plant Sci. 2020;10:1814. [CrossRef].
43. Petitpierre B, Arnold C, Phelps LN, Guisan A. A tale of three vines: current and future threats to wild Eurasian grapevine by vineyards and invasive rootstocks. Divers Distrib. 2023;29(12):1594–608. [CrossRef].
44. Arnold C, Schnitzler A. Ecology and genetics of natural populations of North American Vitis species used as rootstocks in European grapevine breeding programs. Front Plant Sci. 2020;11:866. [CrossRef].
45. Greer DH, Weedon MM. The impact of high temperatures on Vitis vinifera cv. Semillon grapevine performance and berry ripening. Front Plant Sci. 2013;4:491. [CrossRef].
46. Ebadi A, May P, Coombe BG. Effect of short-term temperature and shading on fruit-set, seed and berry development in model vines of V. vinifera, cvs Chardonnay and Shiraz. Aust J Grape Wine Res. 1996;2(1):1–8. [CrossRef].
47. Ristic R, Iland PG. Relationships between seed and berry development of Vitis vinifera L. cv Shiraz: developmental changes in seed morphology and phenolic composition. Aust J Grape Wine Res. 2005;11(1):43–58. [CrossRef].
48. Xiao H, Wang Y, Liu W, Shi X, Huang S, Cao S, et al. Impacts of reproductive systems on grapevine genome and breeding. Nat Commun. 2025;16:2031. [CrossRef].